Differential elastic electron-scattering cross sections of pyrimidine in the energy range between 20 eV and 1 keV

W. Y. Baek, M. U. Bug, and H. Rabus
Physikalisch-Technische Bundesanstalt, Bundesallee 100, 38116 Braunschweig, Germany
(Received 7 May 2014; published 24 June 2014)

Differential elastic electron-scattering cross sections of pyrimidine were absolutely measured for electron energies from 20 eV to 1 keV in the angular range between 5° and 135°. The present results agree with the data of other groups within the experimental uncertainties at scattering angles below 75° while considerable differences among the data were found at higher scattering angles. The experimental values were compared to theoretical values calculated using the modified independent-atom model. The theoretical values reproduce the angular dependence of the experimental differential elastic scattering cross sections qualitatively well for electron energies above 60 eV. The sum of the integral elastic scattering cross sections, obtained by the integration of the differential elastic scattering cross sections, and ionization cross sections predicted by the binary-encounter-Bethe model agree with the previously measured total electron-scattering cross sections of pyrimidine to within 8%.

DOI: 10.1103/PhysRevA.89.062716 PACS number(s): 34.80.Bm

I. INTRODUCTION

It is well established that the biological effect of ionizing radiation is not only dependent on the amount of energy deposition but also on its track structure on a submicrometer scale. Track structure calculations are used to predict the complexity of the radiation damage to DNA, which is one of the key parameters influencing the success probability of the subsequent biological repair mechanisms. The track structure is dominated by secondary electrons that are usually produced in a large number by the primary radiation penetrating tissues. The complete description of the track structure and of the spatial distribution of the energy deposition by ionizing radiation therefore requires the data for the electron-scattering cross sections of the biological medium, i.e., total, singly differential elastic, and doubly differential inelastic electron-scattering cross sections.

Although the relevance of the track structure of secondary electrons at the DNA scale for radiation damage had been recognized for a long time [1–3], the major measurements of the electron-scattering cross sections of the DNA constituents started only several years after Sanche and co-workers [4] demonstrated the importance of low-energy electrons for DNA strand breaks. Since then, a number of experimental and theoretical works have been published with respect to the interaction processes between electrons and the DNA or DNA components. The initial experimental studies on the electron-scattering cross sections of DNA constituents were carried out mainly on tetrahydrofuran, which is commonly used as a substitute for the deoxyribose composing the backbone of the DNA [5–14]. Currently, the focus is shifting to other molecules of biological interest, such as pyrimidine. Pyrimidine ($C_4H_4N_2$) is an aromatic compound with a six-member ring structure belonging to the group of diazine. As the core building block of the nucleobases cytosine and thymine, it is a molecular component of the DNA. Pyrimidine is liquid at room temperature and its vapor pressure at 30 °C is high enough to produce a molecular beam with a sufficiently large density for electron-scattering experiments.

Several experimental electron impact studies on pyrimidine have been carried out in the past 10 years. Ning *et al.* [15] investigated the electronic structure of the valence orbitals of pyrimidine using electron momentum spectroscopy. Buith-Williams [16] studied the ionization dynamics of the outer valence orbitals of pyrimidine by means of the electron-electron coincidence technique. Linert *et al.* [17] measured total ionization cross sections of pyrimidine by collecting fragment ions produced upon electron impact in the energy range between 10 and 145 eV. Mašin *et al.* [18] and Jones *et al.* [19] recently reported integral and differential electronic excitation cross sections of pyrimidine, respectively, for electron energies T between 15 and 50 eV. Total electron-scattering cross sections (TCSs) of pyrimidine were measured by Baek *et al.* [20] and Fuss *et al.* [21] in the energy range from 5 to 1 keV and from 8 to 500 eV, respectively. Differential elastic electron-scattering cross sections (DCSs) of pyrimidine had been reported earlier. Maljković *et al.* [22] experimentally determined elastic DCSs of pyrimidine for scattering angles from 30° to 110° in the energy range between 30 and 300 eV. Palihawadana *et al.* [23] focused their measurement on lower electron energies. They published elastic DCSs of pyrimidine for electron energies between 3 and 50 eV in the angular range mainly from 20° to 129°.

The present article provides elastic DCSs of pyrimidine for wider energy and angular ranges. They have been measured absolutely for electron energies from 20 to 1 keV in the angular range between 5° and 135°. The experimental data are compared to theoretical results that were calculated by employing the modified independent-atom model [24–26].

II. EXPERIMENT

The measurement was carried out using the crossed-beam arrangement and the method which had been described in detail in an earlier paper [14]. Briefly, the elastic DCS $d\sigma_{\mathrm{el}}/d\Omega$ can be determined absolutely using the TCSs σ_t of the respective molecule if the effective interaction volume, i.e., the parts of the interaction volume between the electron and molecular beams from which scattered electrons are detected, do not change with the scattering angle θ. In this case, the ratio of $d\sigma_{\mathrm{el}}/d\Omega$ to σ_t is equal to that of $\Delta N_{\mathrm{el}}/\Delta\Omega$ to the total

count rate N_t of scattered electrons,

$$\frac{d\sigma_{\rm el}(\theta)}{d\Omega} = \sigma_t \frac{\Delta N_{\rm el}(\theta)/\Delta\Omega}{N_t} = \sigma_t \frac{\Delta N_{\rm el}(\theta)/\Delta\Omega}{\Delta I/e}, \qquad (1)$$

where $\Delta N_{\rm el}$ is the count rate of electrons scattered elastically into the solid angle element $\Delta\Omega$, ΔI is the decrease of the electron beam current after the passage of the molecular beam, and e is the electron charge.

The experimental setup consisted of an electron gun, a gas nozzle for the production of a molecular beam, a Faraday cup for the measurement of the electron beam current I, and an electron energy analyzer. All components of the apparatus were assembled within a scattering chamber made of Permalloy. The scattering angle θ was adjusted by means of a turntable on which the electron gun was mounted. The gas nozzle was aligned such that its symmetry axis coincided with the rotation axis of the turntable. Both were mechanically connected to each other in order to avoid the change of the effective interaction volume with the scattering angle. The turntable also carried the Faraday cup that was placed opposite to the electron gun on the other side of the gas nozzle and of a beam monitor. The beam monitor, a channel electron multiplier, was mounted at a fixed angle to the electron beam direction. Its count rate due to electrons scattered by the molecular beam was used to monitor the temporal change of the electron beam current and of the effective interaction volume. The electron energy analyzer was a 180° hemispherical condenser with a mean radius of 150 mm. Electrons passing through the energy analyzer were detected by means of five channel electron multipliers.

The electron beam current varied between 1 and 100 pA depending on the electron energy. The beam current was chosen such that the detector count rate did not exceed 10^4 s^{-1} to avoid a change in the detection efficiency with the count rates that may occur at higher count rates. The energy width [full width at half maximum (FWHM)] of the primary electrons was about 0.5 eV. Pyrimidine was purchased from Aldrich Chemical Ltd. The purity stated by the manufacturer was better than 98%. The vapor pressure of pyrimidine at 25 °C amounts to 22.4 mbar. During the measurement, the room temperature was kept at 30 °C to obtain a sufficient evaporation rate from liquid pyrimidine. The molecular beam was produced by means of a single cylindrical tube 80 mm in length and 2 mm in diameter. The pressure p_r in the reservoir above the molecular beam tube was adjusted to 0.2 mbar. It was measured using a capacitance manometer and could be varied by means of a leak valve situated between the manometer and the bottle containing liquid pyrimidine. At this pressure, the molecular flow rate was about 0.01 mbar l/s, leading to a residual pressure of about 1.5×10^{-5} mbar in the scattering chamber at a pumping speed of 750 l/s. In order to minimize the contamination of the detectors by the organic gas, the electron analyzer was differentially evacuated by an additional turbomolecular pump located close to the exit slit of the analyzer. At a flow rate of 0.01 mbar l/s, the number of molecules per area along the entire path of the primary electron beam is in the order of 10^{13} cm^{-2}. When considering that the integral elastic scattering cross section does not exceed 4×10^{-15} cm^2 in the energy range of interest for this work, the probability for a multiple scattering was lower than 1%. In other words, the single collision condition was fulfilled to a great extent.

For the determination of the elastic DCSs according to Eq. (1), the current loss ΔI and the count rate $\Delta N_{\rm el}/\Delta\Omega$ of electrons scattered elastically have to be measured. To reduce the uncertainties arising due to fluctuations of the electron beam current, the current loss ΔI was at first measured as a function of the pressure p_r in the reservoir above the molecular beam tube. As described in Ref. [14], ΔI increases linearly with p_r. The slope of the line obtained by the best fit to the experimental points ΔI vs p_r was used to calculate the value of ΔI at a given p_r. To determine $\Delta N_{\rm el}/\Delta\Omega$, the detector count rate was recorded as a function of the analyzer pass energy and $\Delta N_{\rm el}/\Delta\Omega$ was defined as the area of the elastic peak in the electron energy spectrum. It is noteworthy that because of the finite energy resolution of the electron energy analyzer and the energy width of primary electrons, the greater part of the rotational and vibrational excitations was not resolved from elastic scattering in this experiment.

As mentioned above, the residual pressure during the measurement amounted to about 1.5×10^{-5} mbar. In order to take into account the additional scattering of electrons by the residual gas molecules, a background measurement was carried out for each energy and scattering angle. In the background measurement, the gas was introduced into the scattering chamber through a wide hole situated about 30 cm above the scattering zone. In this way, a rather homogeneous pressure distribution corresponding to the spatial distribution of the residual gas molecules could be obtained in the scattering zone. The background pressure was adjusted by means of a leak valve located between the hole and the bottle containing the liquid pyrimidine. It was chosen to be as high as the residual pressure produced by the molecular beam. The values of ΔI and $\Delta N_{\rm el}/\Delta\Omega$ obtained with the molecular beam reduced by those determined in the background measurement were then used to calculate the elastic DCSs according to Eq. (1).

III. CALCULATION

The elastic DCSs of pyrimidine were calculated for electron energies between 60 and 1 keV using the modified independent-atom model (MIAM) [24–26]. The method is based upon the independent-atom model, with the difference being that the MIAM additionally takes into account the multiple scattering of electrons inside the molecule and the scattering due to long-range potentials. In the case of tetrahydrofuran, it could well reproduce the angular dependence of the experimental elastic DCSs for electron energies above 60 eV. At energies higher than 600 eV, the values calculated using the model agreed with the measured data mostly to within 10% over the whole angular range [14]. Since the details of the method have been explained in Ref. [14], it is only briefly described here. In the MIAM, the elastic DCS is expressed as the sum of seven terms:

$$\frac{d\sigma_{\rm el}}{d\Omega} = I_L + I_{LS} + I_S + I_{SS} + I_{SD}^{(1)} + I_{SD}^{(2)} + I_{DD}^{(0)}. \qquad (2)$$

The first term I_L is the contribution of the correlation-polarization potential to the elastic scattering and I_{LS} can be

interpreted as the contribution of the coherent scattering taking place between the correlation-polarization potential and the short-range potentials centered at the atoms composing the molecule. The term I_S, the independent-atom model term, is equal to the sum of the elastic DCSs of the individual atoms and I_{SS} originates from the coherent scattering of the incident electron wave between the atoms of the molecule. The subsequent three terms represent the contributions of different grades of multiple scattering occurring within the molecule. The terms $I_{SD}^{(1)}$ and $I_{SD}^{(2)}$ are contributions of two kinds of interference between single and double scattering, and $I_{DD}^{(0)}$ arises due to pure double scattering [24].

The terms on the right-hand side of Eq. (2) are functions of the scattering amplitude and of the coordinates of the atoms in the molecule. The coordinates of the atoms were calculated by means of the quantum chemical program GAUSSIAN 09 [27] deploying the 6-311G** basis set. The scattering amplitudes were calculated using the partial-wave expansion method. The phase shifts of the partial waves were obtained by the solution of the time-independent radial Schrödinger equation for each atom where a complex optical potential [28], defined as the sum of the short-range electrostatic, local exchange, and imaginary absorption potential, was used as the interaction potential. The correlation-polarization potential was set equal to the correlation potential [29] in the region with electron densities higher than a threshold value and to the Buckingham potential [28] elsewhere. For the Buckingham potential, a value of 8.79×10^{-24} cm^3 was used for the mean molecular polarizability of pyrimidine [30,31]. It is noteworthy that the correlation potential was obtained using the local-density approximation and the electron densities were calculated by means of GAUSSIAN 09 [27] deploying the same basis set as above. Assuming that the correlation-polarization potential is generated by a single polarization center, the time-independent radial Schrödinger equation was solved for this potential to obtain the phase shifts of the partial waves and subsequently the scattering amplitude. This scattering amplitude was then used for the calculation of I_L and I_{LS}. The details about the derivation of the interaction potential are also given in Ref. [14].

IV. RESULTS AND DISCUSSION

The results of the measurement and theoretical calculations are shown in Fig. 1 and listed in Table I. The relative uncertainties of the present results amount to 15%. Individual uncertainty sources and the determination of the overall uncertainty have been described in Ref. [14]. The present results agree well with the data of Palihawadana *et al.* [23] for 20 eV electrons. The differences between both data are in the order of the experimental uncertainties. For 30 eV electrons, this measurement well reproduces the results of Palihawadana *et al.* [23] at scattering angles below 90° while there are significant deviations between both data at higher scattering angles. At this energy, the elastic DCSs measured by Palihawadana *et al.* [23] steeply rise with an ascending scattering angle in the angular region of above 90°, leading to a growing deviation from the present data with an increasing scattering angle. At 120°, the data of Palihawadana *et al.* [23] are a factor of about 3.5 higher than the present result. It should be noted, however, that this steep elevation of the elastic DCSs is rather peculiar as such an angular dependence appears neither at lower nor at higher electron energies.

The present results show a good agreement with the data of Maljković *et al.* [22] for 100 eV electrons. Both data almost coincide within the experimental uncertainties over the whole published angular range. For 200 and 300 eV electrons, both data agree within the experimental uncertainties at scattering angles of lower than 45° while the results of this work tend to be higher than those of Maljković *et al.* [22] at greater scattering angles. At these energies, the difference between both data also rises with an increasing scattering angle in the angular range above 45°. The greatest difference was found for 200 eV electrons. The present results show a flat tail towards higher scattering angles at an electron energy of 200 eV as well as of 300 eV, while the elastic DCSs of Maljković *et al.* [22] for 200 eV electrons exhibit a clearly monotonically decreasing angular dependence at high scattering angles, in contrast to their data for 100 and 300 eV electrons.

It is remarkable that the experimental data show a shoulder-like structure in the angular range between 20° and 60°. This structure can also be seen in the data of Maljković *et al.* [22] and of Palihawadana *et al.* [23]. It tends to shift towards lower angles with increasing electron energy. In general, the elastic DCSs monotonically decrease with an increasing scattering angle at electron energies above 200 eV. At lower energies, they form a minimum at scattering angles around 90° to increase towards the backward scattering angle of 180°. As usual, the difference in the elastic DCSs between the forward and backward scattering direction rises with increasing electron energy. While the ratio of the elastic DCS at 5° and 135° is about 10^4 in the case of 1 keV electrons, that in the case of 30 eV electrons amounts to about 10^2.

It can be seen from Fig. 1 that the results of the theoretical calculations match the experimental values to almost within the experimental uncertainties over the whole angular range for electron energies above 600 eV. The difference between both data increases with decreasing electron energy. At lower energies, the theoretical calculations seem to overestimate the elastic DCSs but still reproduce the angular dependence of the present measurement qualitatively well. It is noteworthy that the theoretical results verify the presence of the shoulderlike structure observed in the experimental data. Both data show this structure nearly at the same scattering angles, agreeing in the shift of the structure towards lower scattering angles with increasing electron energy. Furthermore, the theoretical values also predict the minimum appearing at around 90° at electron energies below 100 eV.

It is evident from Fig. 1 that the independent-atom model, represented by the term I_S, provides a good approximation for the elastic DCSs at electron energies above 600 eV, with the exception of scattering angles below 7.5°. The deviation between the theoretical and experimental data at low scattering angles nearly vanishes when taking into account the contributions of the correlation polarization potential and of the coherent scattering represented by the terms I_L, I_{LS}, and I_{SS}, respectively. At high energies, these three terms lead to a considerable increase of the elastic DCS in the forward direction but have only a minor influence on it at

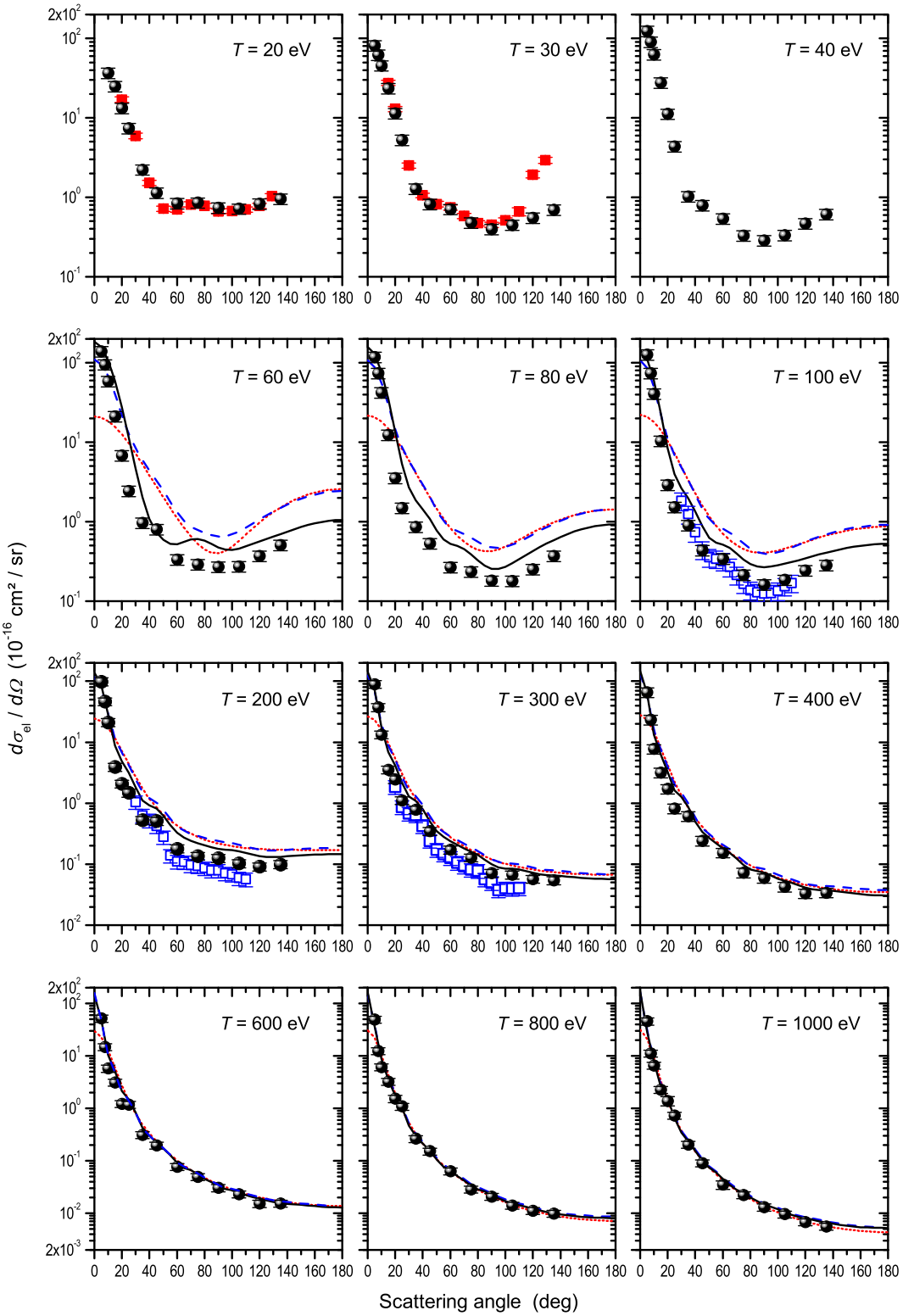

FIG. 1. (Color online) Elastic DCSs of pyrimidine for different electron energies T. Symbols represent experimental data of different groups: ●, present results; ■, Palihawadana *et al.* [23]; □, Maljković *et al.* [22]. The dotted, dashed, and solid lines depict theoretical values corresponding to I_S, $I_L+I_{LS}+I_S+I_{SS}$, and the sum of all terms on the right-hand side of Eq. (2), respectively.

large scattering angles. The angular range where the three terms significantly influence the elastic DCS widens with increasing electron energy. A detailed analysis reveals that the coherent scattering term I_{SS} is responsible for the shoulderlike structure appearing in the angular range between 20° and 60°. Figure 1 furthermore shows that the contribution of multiple scattering, corresponding to the difference between the solid and dashed line, increases with decreasing electron energy. For

TABLE I. Elastic DCSs of pyrimidine in units of 10^{-16} cm^2/sr. Numbers in parentheses are powers of 10 that multiply the cross sections. The relative uncertainties of the tabulated data amount to 15%.

	Electron energy (eV)						
Scattering angle (deg)	20	30	40	60	80	100	200
5		80.98	123.9	138.7	118.0	126.1	98.30
7.5		62.28	90.47	95.16	74.36	74.07	46.49
10	36.55	45.53	62.82	58.68	42.23	40.63	21.10
15	24.86	23.48	27.71	21.11	12.38	10.33	3.912
20	13.31	11.44	11.22	6.790	3.526	2.911	2.076
25	7.402	5.282	4.359	2.439	1.485	1.521	1.476
35	2.239	1.274	1.015	0.964	0.862	0.902	0.527
45	1.142	0.822	0.796	0.805	0.532	0.435	0.510
60	0.838	0.709	0.541	0.333	0.267	0.342	0.179
75	0.855	0.477	0.303	0.290	0.234	0.214	0.136
90	0.741	0.398	0.287	0.269	0.181	0.161	0.125
105	0.718	0.449	0.335	0.273	0.180	0.185	0.102
120	0.829	0.550	0.468	0.370	0.252	0.242	9.08(−2)
135	0.953	0.698	0.611	0.508	0.369	0.284	9.88(−2)

	Electron energy (eV)				
Scattering angle (deg)	300	400	600	800	1000
5	89.51	65.88	51.75	49.35	45.71
7.5	37.37	23.30	14.91	12.40	11.09
10	13.33	7.739	5.750	6.081	6.572
15	3.541	3.167	3.124	3.254	2.277
20	2.458	1.713	1.225	1.524	1.389
25	1.112	0.817	1.176	1.086	0.730
35	0.783	0.613	0.311	0.263	0.203
45	0.349	0.242	0.198	0.152	9.02(−2)
60	0.172	0.154	7.73(−2)	6.29(−2)	3.50(−2)
75	0.128	7.25(−2)	4.92(−2)	2.87(−2)	2.24(−2)
90	7.11(−2)	5.90(−2)	3.03(−2)	2.08(−2)	1.30(−2)
105	6.70(−2)	4.26(−2)	2.31(−2)	1.41(−2)	9.60(−3)
120	5.71(−2)	3.31(−2)	1.52(−2)	1.12(−2)	6.81(−3)
135	5.40(−2)	3.40(−2)	1.54(−2)	9.87(−3)	5.59(−3)

electron energies higher than 600 eV, the influence of multiple scattering on the elastic DCS is negligibly small.

Apart from the DCSs, the integral elastic scattering $\sigma_{\rm el}$ and momentum-transfer cross section σ_m are of importance for electron transport calculations. They were therefore computed by the integration of $d\sigma_{\rm el}/d\Omega$ and $(1-\cos\theta)d\sigma_{\rm el}/d\Omega$, respectively, over the whole solid angle, where the differential solid angle element was given by $2\pi\sin\theta d\theta$ due to the independence of the elastic DCS on the azimuth angle in this experiment. The calculation was carried out using the present experimental data listed in Table I. For electron energies above 60 eV, the values for scattering angle ranges 0°–5° and 135°–180° were obtained by the extrapolation of the measured data using the angular dependences of the theoretical DCSs depicted in Fig. 1. The calculation of $\sigma_{\rm el}$ and σ_m for the electron energies below 60 eV was calculated using the molecular phase-shift analysis technique of Tanaka *et al.* [32]. The relative overall uncertainty of $\sigma_{\rm el}$ and σ_m was estimated to be 18% for electron energies above 60 eV and 21% below 60 eV.

Figure 2 shows $\sigma_{\rm el}$ of pyrimidine together with its ionization cross sections σ_i and TCSs σ_t [20,21]. The dash-dotted line represents ionization cross sections calculated using the binary-encounter-Bethe (BEB) model [33]. The input parameters of the BEB model, such as the binding energies and the mean kinetic energies of electrons in the molecular orbitals, were determined by means of the program GAUSSIAN 09 [27] deploying the 6-311G** basis set. In Fig. 2, the experimental TCSs σ_t are compared to the sum $\tilde{\sigma}_t = \sigma_{\rm el} + \sigma_i$, where σ_i was calculated using the BEB model [33]. It can be seen from Fig. 2 that $\tilde{\sigma}_t$ almost exactly reproduces the earlier experimental results [20] of the present group for electron energies above 60 eV and agrees with the results of Fuss *et al.* [21] within the experimental uncertainties. The good agreement between σ_t and $\tilde{\sigma}_t$, despite disregarding the excitation cross section $\sigma_{\rm ex}$, suggests that $\sigma_{\rm ex}$ is significantly smaller than $\sigma_{\rm el}$ and σ_i above 60 eV.

The excitation of a molecule by electron impact can occur by rotational, vibrational, and electronic transitions. Unfortunately, the available cross-section data for the electron impact excitations of pyrimidine are very scarce. As far as we know, electronic excitation cross sections of pyrimidine have been experimentally determined only by Jones *et al.* [19]. They measured differential electronic excitation cross

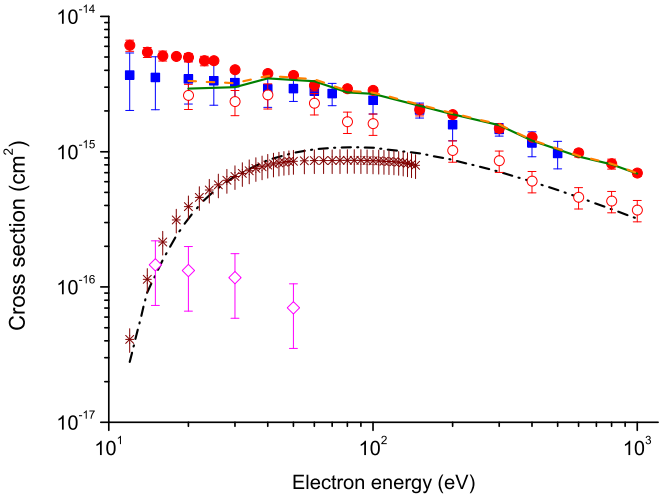

FIG. 2. (Color online) Electron scattering cross sections of pyrimidine: ○, integral elastic scattering cross section σ_{el} determined in the present work; *, ionization cross section σ_i measured by Linert *et al.* [17]; ◊, experimental electronic excitation cross section of Jones *et al.* [19]; ■, experimental TCSs of Fuss *et al.* [21]; ●, TCSs measured earlier by the present group [20]; – · – · –, ionization cross section σ_i predicted by the BEB model [33];—, sum of σ_{el} and σ_i predicted by the BEB model [33]; – – –, sum of σ_{el}, σ_i, and the integral rotational excitation cross section $\Delta\sigma_{rot}$ over the nonmeasured angular ranges.

sections of pyrimidine for electron energies T from 15 to 50 eV and obtained σ_{ex} by the integration of the differential excitation cross section over the scattering angle. It amounted to 0.7×10^{-16} or 0.87×10^{-16} cm^2 for 50 eV electrons, depending on the method used for the extrapolation of the experimental data beyond the measured angular range. Experimental data for the vibrational excitation cross sections of gaseous pyrimidine is still lacking. As far as we can tell, the only published experimental data for the vibrational excitation cross sections of pyrimidine stem from the measurement by Levesque *et al.* [34], who determined the cross sections of condensed pyrimidine for five vibrational transitions in the electron energy range between 2 and 12 eV. According to their measurement, the cross sections for the five main vibrational excitations are in the order of 10^{-17} cm^2 at an electron energy of 12 eV.

TABLE II. Integral cross sections of pyrimidine for elastic scattering σ_{el}, momentum transfer σ_m, ionization σ_i, and total electron-scattering cross section σ_t in units of 10^{-16} cm^2. The ionization cross section σ_i were calculated using the BEB model [33] and σ_t had been measured earlier by the present group [20]. The relative uncertainties of σ_{el} and σ_m were estimated to be 18% for electron energies above 60 eV and 21% below 60 eV.

Electron energy (eV)	σ_{el}	σ_m	σ_i	σ_t
20	26.04	13.47	3.22	49.69
30	23.42	9.828	6.62	40.26
40	26.20	7.736	8.66	37.71
60	22.82	5.638	10.4	30.80
80	16.64	4.059	10.8	29.09
100	16.08	3.450	10.7	28.32
200	10.19	1.686	8.70	18.73
300	8.556	1.178	7.12	14.82
400	6.050	0.819	6.01	12.76
600	4.600	0.482	4.61	9.775
800	4.313	0.361	3.76	8.127
1000	3.701	0.244	3.19	6.942

The results of Jones *et al.* [19] and Levesque *et al.* [34] show that both the electronic [19] and vibrational [10] excitation cross sections decrease with increasing electron energy above 10 eV. Based on the two experimental results and the assumption that vibrational excitation cross sections of gaseous pyrimidine is not noticeably different from those of condensed pyrimidine, the electronic and vibrational excitation cross sections at the electron energy of 50 eV were here estimated to be about one order of magnitude smaller than the ionization cross section predicted by the BEB model [33]. Moreover, it is to be expected that the ratio of excitation to ionization cross section decreases with increasing electron energy and approaches zero at high electron energies. To sum up, electronic and vibrational excitation cross sections play only a minor role compared to other interaction cross sections at energies above 60 eV.

In the case of molecules with high dipole moments as pyrimidine, rotational transitions lead to a strong elevation of the excitation cross section, especially at small scattering angles. In the measured angular range, rotational excitation cross sections need not be taken into account in the calculation of $\tilde{\sigma}_t$, because rotational excitations could not be discriminated against elastic scattering due to the finite-energy resolving power of the electron energy analyzer and are consequently included in σ_{el}. Following the method described in an earlier work [20], the contribution $\Delta\sigma_{rot}$ of rotational excitations to electron scattering beyond the measured angular range was estimated using the formula of Collins and Norcross [35] for the differential rotational excitation cross section $d\sigma_{rot}/d\Omega$, which is based on the first Born approximation for a rotating dipole, and 2.28 D [36] for the value of the dipole moment of pyrimidine. The energy levels of the rotational states of pyrimidine required for this estimate were calculated by means of the computational method described in Ref. [37]. The value of $\Delta\sigma_{rot}$ was obtained by summing up the integrals of $d\sigma_{rot}/d\Omega$ over the nonmeasured angular ranges 0°–5° and 135°–180°. In the case of 20 eV electrons, the integration was carried out over the angular ranges 0°–10° and 135°–180°. It is noteworthy that the integral of $d\sigma_{rot}/d\Omega$ over the angular range 0°–5° makes up more than 95% of $\Delta\sigma_{rot}$. It can be seen from Fig. 2 that small-angle electron scattering due to rotational excitations noticeably contributes to the TCSs of pyrimidine at electron energies below 60 eV. At 20 eV, $\Delta\sigma_{rot}$ amounts to about 8% of the TCS of pyrimidine.

Since excitation cross sections of pyrimidine play only a minor role above 60 eV, the good agreement between σ_t and $\tilde{\sigma}_t$ means that the ionization cross sections of pyrimidine predicted by the BEB model [33] are consistent with the experimental results of the present group for σ_{el} and σ_t. A worse agreement between σ_t and $\tilde{\sigma}_t$, albeit borderline when considering the uncertainties, was found if the latter was calculated using the ionization cross sections measured by Linert *et al.* [17]. Figure 2 shows that at

high energies, the interaction of pyrimidine with electrons is nearly equally partitioned between elastic scattering and ionization.

V. CONCLUSION

The present experimental data for the elastic DCSs of pyrimidine agree reasonably well with the results of other groups [22,23] at scattering angles below 75°, whereas considerable differences were found at higher scattering angles. The result of Palihawadana *et al.* [23] for 30 eV electrons at 120° is about three times higher than found in this work. In contrast, the data of Maljković *et al.* [22] tend to be lower than the present results at scattering angles above 75°.

The experimental data of this work agree well with the theoretical values obtained using the MIAM [24–26] at electron energies above 600 eV. The differences between both data at high energies are smaller than the experimental uncertainties. At lower energies, the theoretical model seems to overestimate the elastic DCSs on the absolute scale, but reproduces the angular dependence of the experimental data qualitatively well. For electron energies above 60 eV, the sum of the integral elastic scattering and ionization cross section, calculated by means of the BEB model [33], agrees with the TCSs of pyrimidine [20,21] within the experimental uncertainties. This good agreement is evidence of the realistic prediction of ionization cross sections by the BEB model [33] above 60 eV, implying that integral elastic scattering cross sections, when data are not available, may be derived from the TCSs and the calculated ionization cross sections.

ACKNOWLEDGMENTS

This work was carried out within the EMRP joint research project BioQuaRT. The EMRP is jointly funded by the EMRP participating countries within EURAMET and the European Union.

[1] D. E. Charlton and J. L. Humm, Int. J. Radiat. Biol. **53**, 353 (1988).
[2] D. E. Charlton, H. Nikjoo, and J. L. Humm, Int. J. Radiat. Biol. **56**, 1 (1989).
[3] D. T. Goodhead, Int. J. Radiat. Biol. **65**, 7 (1994).
[4] B. Boudaïffa, P. Cloutier, D. Hunting, M. A. Huels, and L. Sanche, Science **287**, 1658 (2000).
[5] A. Zecca, C. Perazzolli, and M. J. Brunger, J. Phys. B **38**, 2079 (2005).
[6] A. R. Milosavljević, A. Giuliani, D. Šević, M.-J. Hubin-Franskin, and B. P. Marinković, Eur. Phys. J. D **35**, 411 (2005).
[7] M. Fuss, A. Muñoz, J. C. Oller, F. Blanco, D. Almeida, P. Limão-Vieira, T. P. D. Do, M. J. Brunger, and G. García, Phys. Rev. A **80**, 052709 (2009).
[8] P. Możejko, E. Ptasínska-Denga, A. Domaracka, and C. Szmytkowski, Phys. Rev. A **74**, 012708 (2006).
[9] M. Allan, J. Phys. B **40**, 3531 (2007).
[10] C. J. Colyer, V. Vizacaino, J. P. Sullivan, M. J. Brunger, and S. J. Buckman, New J. Phys. **9**, 41 (2007).
[11] M. Dampc, A. R. Milosavljević, and M. Zubek, Chem. Phys. Lett. **443**, 17 (2007).
[12] T. P. T. Do, M. Leung, M. Fuss, G. García, F. Blanco, K. Ratnavelu, and M. J. Brunger, J. Chem. Phys. **134**, 144302 (2011).
[13] A. Gauf, L. R. Hargreaves, A. Jo, J. Tanner, M. A. Khakoo, T. Walls, C. Winstead, and V. McKoy, Phys. Rev. A **85**, 052717 (2012).
[14] W. Y. Baek, M. Bug, H. Rabus, E. Gargioni, and B. Grosswendt, Phys. Rev. A **86**, 032702 (2012).
[15] C. G. Ning, K. Liu, Z. H. Luo, S. F. Zhang, and J. K. Deng, Chem. Phys. Lett. **476**, 157 (2009).
[16] J. D. Builth-Williams, S. M. Bellm, D. B. Jones, H. Chaluvadi, D. H. Madison, C. G. Ning, B. Lohmann, and M. J. Brunger, J. Chem. Phys. **136**, 024304 (2012).
[17] I. Linert, M. Dampc, B. Mielewska, and M. Zubek, Eur. Phys. J. D **66**, 20 (2012).
[18] Z. Mašín, J. D. Gorfinkiel, D. B. Jones, S. M. Bellm, and M. J. Brunger, J. Chem. Phys. **136**, 144310 (2012).
[19] D. B. Jones, S. M. Bellm, F. Blanco, M. Fuss, G. García, P. Limão-Vieira, and M. J. Brunger, J. Chem. Phys. **137**, 074304 (2012).
[20] W. Y. Baek, A. Arndt, M. U. Bug, H. Rabus, and M. Wang, Phys. Rev. A **88**, 032702 (2013).
[21] M. C. Fuss, A. G. Sanz, F. Blanco, J. C. Oller, P. Limão-Vieira, M. J. Brunger, and G. García, Phys. Rev. A **88**, 042702 (2013).
[22] J. B. Maljković, A. R. Milosavljević, F. Blanco, D. Šević, G. Garcia, and B. P. Marinković, Phys. Rev. A **79**, 052706 (2009).
[23] P. Palihawadana, J. Sullivan, M. Brunger, C. Winstead, V. McKoy, G. Garcia, F. Blanco, and S. Buckman, Phys. Rev. A **84**, 062702 (2011).
[24] S. Hayashi and K. Kuchitsu, J. Phys. Soc. Jpn. **41**, 1724 (1976).
[25] A. Jain, J. Phys. B **15**, 1533 (1982).
[26] A. Jain and S. S. Tayal, J. Phys. B **15**, L867 (1982).
[27] GAUSSIAN 09, Gaussian, Inc., Wallingford, CT.
[28] F. Salvat, Phys. Rev. A **68**, 012708 (2003).
[29] N. T. Padial and D. W. Norcross, Phys. Rev. A **29**, 1742 (1984).
[30] C. Hattig, O. Christiansen, S. Coriani, and P. Jorgensen, J. Chem. Phys. **109**, 9237 (1998).
[31] B. Jansik, D. Jonsson, P. Salek, and H. Agren, J. Chem. Phys. **121**, 7595 (2004).
[32] H. Tanaka, T. Okada, L. Boesten, T. Suzuki, T. Yamamoto, and M. Kubo, J. Phys. B **15**, 3305 (1982).
[33] Y.-K. Kim and M. E. Rudd, Phys. Rev. A **50**, 3954 (1994).
[34] P. L. Levesque, M. Michaud, and L. Sanche, J. Chem. Phys. **122**, 094701 (2005).
[35] L. A. Collins and D. W. Norcross, Phys. Rev. A **18**, 467 (1978).
[36] P. Chen and R. A. Holroyd, J. Phys. Chem. **100**, 4491 (1996).
[37] A. Jain and D. G. Thompson, Comput. Phys. Commun. **30**, 301 (1983).